



Deposited via The University of Sheffield.

White Rose Research Online URL for this paper:

<https://eprints.whiterose.ac.uk/id/eprint/131666/>

Version: Accepted Version

Article:

Selvaraj, N.B., Fernandes, M., Reaney, I.M. et al. (2018) Linking sintering stresses to nano modification in the microstructure of BaLa₄Ti₄O₁₅ by transmission electron microscopy. *Materials Characterization*, 142. pp. 1-8. ISSN: 1044-5803

<https://doi.org/10.1016/j.matchar.2018.04.054>

Reuse

This article is distributed under the terms of the Creative Commons Attribution-NonCommercial-NoDerivs (CC BY-NC-ND) licence. This licence only allows you to download this work and share it with others as long as you credit the authors, but you can't change the article in any way or use it commercially. More information and the full terms of the licence here: <https://creativecommons.org/licenses/>

Takedown

If you consider content in White Rose Research Online to be in breach of UK law, please notify us by emailing eprints@whiterose.ac.uk including the URL of the record and the reason for the withdrawal request.

(revised version paper MATERIALSCHAR_2017_2819, January 2018)

**Linking sintering stresses to nano modification in the microstructure of
BaLa₄Ti₄O₁₅ by transmission electron microscopy**

Abstract

High quality factor and a temperature stable resonant frequency make BaLa₄Ti₄O₁₅ (BLT) ceramics attractive materials for microwave applications. Aiming to exploit the effects of external stresses on the development of textured and anisotropic microstructures to optimise MW properties, the influence of applied external pressure during sintering of BLT ceramics is analysed. HRTEM and geometric phase analysis (GPA) showed that stresses applied during sintering, trigger the nucleation and growth of faults hypothesised to be due to the errors in the AO₃ layer (basal plane) stacking sequence of the hexagonal perovskite structure. The results reveal a strong correlation between the high concentration of structural defects and the development of anisotropic microstructures, which tune the properties of BLT. Stresses applied during sintering are therefore a promising tool to design material properties.

Key words:

stress, sintering, barium lanthanum titanate, high resolution transmission electron microscopy, microstructure, geometric phase analysis

Introduction

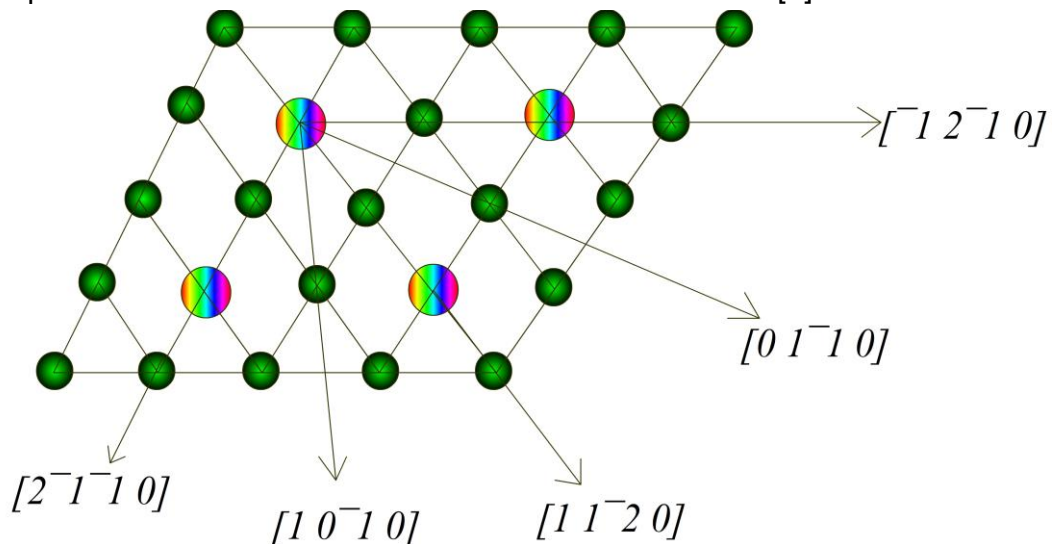
Advances during the last few decades in microwave (MW) technology have brought a revolution in telecommunication systems. The main criteria for the use of microwave materials in devices are compactness, low loss and reliability. The size of a MW component may be reduced by utilising high permittivity (ϵ_r) ceramics since the resonant frequency of a MW material is inversely proportional to ϵ_r . This is particularly important for dielectrically loaded Global Positioning Systems (GPS) antennas in handheld devices where space within the device casing is at a premium. However, for resonators and cavity filters in base stations the main technological driving force is the selectivity of the material to a narrow frequency range to maximise the usage of limited sections of the Electromagnetic (EM) MW spectrum and thus the MW quality factor (Q_f) dominates innovation. Low temperature co-fired ceramic (LTCC) technology is used to create integrated MW circuits in which the EM radiation propagates through a sequence of waveguiding channels and filters embedded in ceramic layers [1]. In this technology, low cost and compatibility with Ag electrodes are critical.

Despite these diverse applications, one unifying material property is critical to all MW materials. The temperature coefficient of the resonant

frequency (τ_f) must be close to zero. For modern cavity resonators and filters, the most stringent application for materials, $\tau_f = \pm 1$ ppm/ $^{\circ}\text{C}$, $Qf > 40,000$ GHz and $20 \geq \epsilon_r \geq 50$. For dielectrically loaded antenna the requirements for τ_f and Qf are relaxed since loss is dominated by the ceramic/metallisation interface, $\tau_f = \pm 10$ ppm/ $^{\circ}\text{C}$, $20 \geq \epsilon_r \geq 100$, $Qf = 10,000$ GHz, and for LTCC the presence of metallisations within the structure limits the Qf of the device, $\tau_f \pm 10$ ppm/ $^{\circ}\text{C}$ $Qf < 1000$ GHz, and $8 \geq \epsilon_r \geq 100$ [2].

There is considerable interest in titanate based electroceramics for microwave applications due to their exceptional dielectric properties [3-6]. Amongst titanate-based materials, compositions in BaO - Re₂O₃ - TiO₂ family are widely used in a broad range of applications such as dielectric resonators, microwave substrates for antennas and C0G (Electronic Industries Alliance standard for temperature compensating class 1 capacitors) temperature stable capacitors. There are many materials used for dielectric resonators but where a combination of medium to high permittivity is required with selectivity to a narrow frequency range, compositions based on BaLa₄Ti₄O₁₅ (BLT) are commercially competitive with MW properties reported as $\epsilon_r \sim 45$, $Qf \sim 41000$ and $\tau_f \sim -26$ ppm/ $^{\circ}\text{C}$.

BLT has a B-site deficient layered perovskite structure with a hexagonal P3c1 space group [5,6] (Figure 1). AO₃ mixed layers are stacked to form the layered perovskite structure and the distance between these layers influences the properties of BLT [5,6]. Common crystal imperfections in such structures are stacking faults, which occur due to the disparities in stoichiometry of the AO₃ layers. The hexagonal structure of BLT essentially arises because at least two octahedral layers are face shared in contrast with cubic perovskites in which all octahedra are corner shared [7].



Schematic views of the AO₃ mixed layers packing in BLT: arrangement of A and O atoms in the AO₃ mixed layers.

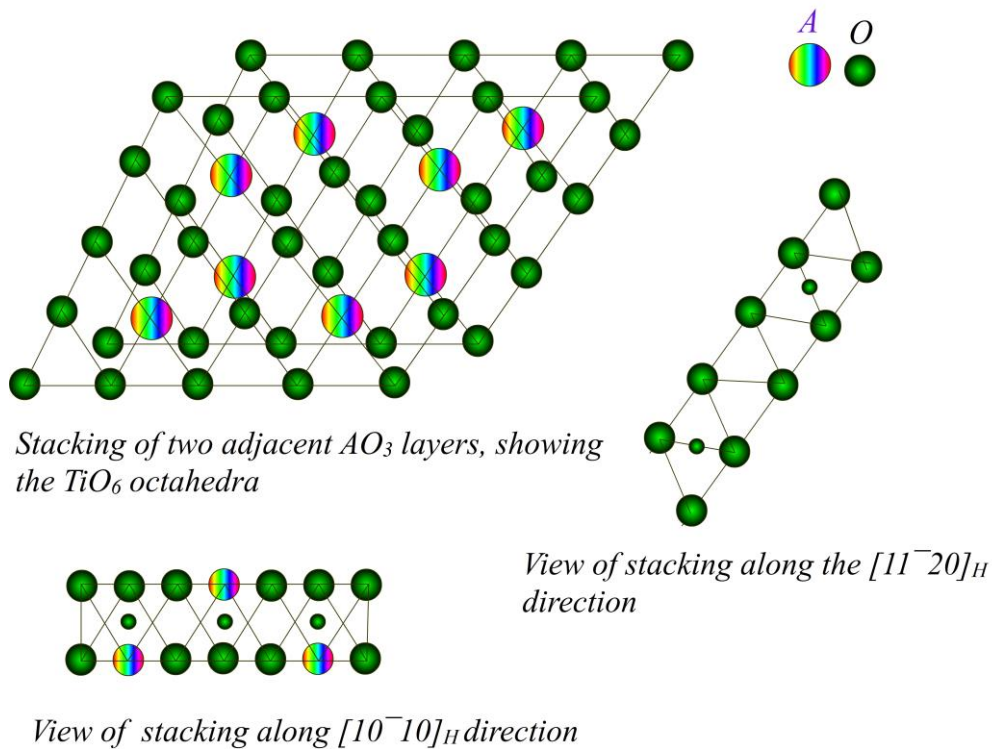


Figure. 1 Schematic representation of the layered perovskite structure of BLT in which A represents Ba and La ions in the structure [7,8]. The BLT structure exhibits some layers in which the octahedra are face rather than corner shared [7].

To control MW properties, it is imperative that ceramics attain an optimised microstructure. There have been several attempts to control the dielectric properties of microwave materials by using sintering variables, [3, 4]. Temperature, heating/cooling rates and sintering atmospheres have been frequently used in titanates to change the microstructure and thus the dielectric properties [5]. In $SrTiO_3$, two sintering regimes exist and a slight variation in composition is enough to change the microstructure. The low temperature regime is dominated by grain boundary diffusion and at high temperature volume diffusion occurs [5]. In addition, depending on Sr/Ti stoichiometry the densification and microstructure may vary [5]. We have recently shown that a grain boundary (GB) anomaly can be triggered in $SrTiO_3$ by varying the sintering temperature [9]. Literature reports that in $SrTiO_3$ the grain growth anomaly may result from changes in grain boundary structure and stoichiometry with modification of the sintering temperature leading to changes in the grain boundary energy and/or mobility [10]. A TEM study on the grain boundary stoichiometry of $SrTiO_3$ [11] reports that Ti rich grain boundary regions diffuse slower than others, but no clear correlation to the grain growth anomaly has yet been obtained. The microstructure of ceramics is also controlled by the sintering atmosphere. For example, during

the sintering of titanates at high temperature where reduction of Ti^{4+} may occur high oxygen partial pressure is utilized to maintain O stoichiometry.

Another way to control materials microstructure is by applying external stresses during the sintering. In functional thin films the role of stress is well known and used as an engineering tool to induce new physical phenomena. In $SrTiO_3$ thin films for example, ferroelectric behaviour may be induced through compressive in-plane strain [12]. However, the effect of stresses in the microstructure development of ceramics is not so well known and rarely documented. Since Abouaf *et al* [13,14] first studied hot isostatic pressing of Al_2O_3 and observed that crystal imperfections are formed during sintering under stress, which relates to abnormal grain growth, no other systematic investigations have been conducted. Recently, however, Zhi *et al* [15] and Amaral *et al.* [16] reported a marked effect of the mechanical stress on the microstructural development arising from the substrate during the constrained sintering of $BaNd_2Ti_5O_{14}$ (BNT) and BLT thick films. Zhi *et al* [15] and Amaral *et al* [16] hypothesized that tensile compatibility stresses induced by the geometrical constraint increase the mobility of grain boundaries or the driving force for grain boundary transport enhancing grain growth. However, a comprehensive understanding of the effect of stresses on the microstructure during sintering and its role and/or utilisation in the development/design of textured and anisotropic microstructures, is still missing.

In this work we link the microstructural changes in BLT ceramics to the external pressure applied during sintering. To this end, systematic HRTEM studies were conducted on BLT ceramics sintered under pressure and without external stresses with the results being used to develop a mechanistic understanding of the role of stress in sintering.

Experimental

Single phase $BaLa_4Ti_4O_{15}$ (BLT) powders, with 3 μm average particle size, were prepared through conventional solid state route by mixing the stoichiometric proportion of $BaCO_3$ - La_2O_3 - TiO_2 (<99% purity, Merck) powders, in ethanol, and ball milling, for 24 h, in a Teflon jar before and after calcination at 1330 $^{\circ}C$, for 3 h. Phase purity of the BLT powders were ensured with XRD. Powders were thermal consolidated by hot pressing (HP) in a hot press furnace (homemade by UIDM, Viana do Castelo) as schematically shown in Figure 2. Alumina dies and punches were used and the thermal cycle conditions leading to near dense samples were: a constant heating rate of 8 $^{\circ}C\ min^{-1}$ up to a maximum temperature of 1250 $^{\circ}C$, for 2 h, and 65 MPa of applied pressure. For a systematic and comparative study of the pressure sintering effect, pressed powder compacts were also densified by the conventional sintering (CS) method, without external pressure. In this case, to attain high dense compacts, a maximum temperature of 1530 $^{\circ}C$, for 3 h, was used. Polished and thermally etched fracture surfaces (at 1480 $^{\circ}C$ for 60 s) of the sintered samples were first inspected by scanning electron microscopy

(SEM, Hitachi S-4100) to have the general knowledge on the morphological details and to check phase purity with energy dispersive X-ray spectroscopy (EDS). SEM images were analysed using Image J software.

For transmission electron microscopy (TEM) studies both CS and HP ceramics were thinned down to 20 μm by polishing using tungsten grid paper followed by diamond pastes and made electron transparent using precision the ion polishing system (PIPS-Model 691; Gatan, Pleasanton, CA); TEM studies were done using Hitachi 9000; High resolution TEM (HRTEM) studies were performed with SACTEM TECNAI-F20 microscope in CEMES, Toulouse.

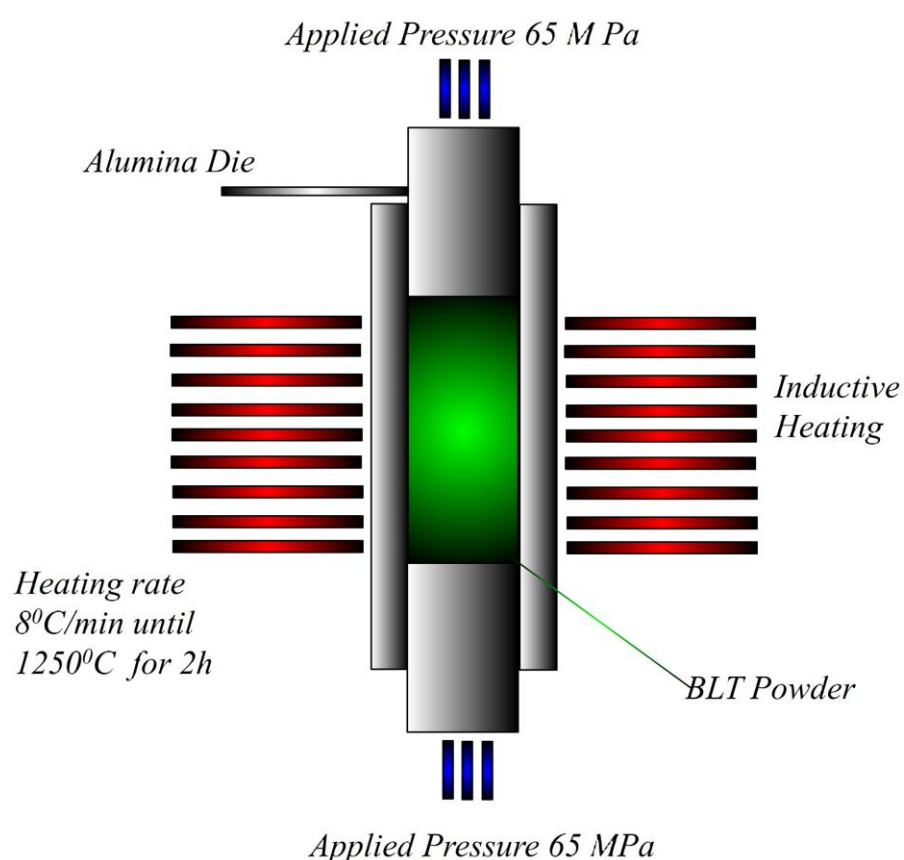


Figure 2. Schematic of the preparation of HP BLT ceramics

In this work, geometric phase analysis (GPA) was used to investigate structural modifications by applied external stress during sintering, following the difference in fringe width. The Hytch method [18-22] was used to perform GPA, taking information from the deformation of the lattice fringes to create the maps of displacement and strain fields, **lattice strain analysis using GPA is an accurate method, which could be done in atomic resolutions [23]**. These maps are based on the Fourier analysis of a HRTEM lattice image, selecting a strong Bragg reflection and performing an inverse Fourier transform. The

phase component of the resulting complex image gives information on the local displacements of the atomic planes. In short, the procedure of GPA is as follows, where a perfectly periodic set of fringes can be represented by a cosine function:

$$I(x) = A \cos(2\pi g_0 x + \phi(x)) \quad [1]$$

here g_0 is the frequency of the fringe and $\phi(x)$ a spatially varying phase value which will include the slight spatial variations in the fringe periodicities. This phase term can be rewritten as a function of the frequency g_0 and the displacement of the non-regular fringes from their ideal periodic position, $u(x)$:

$$\phi(x) = 2\pi g_0 u(x) \quad [2]$$

that is

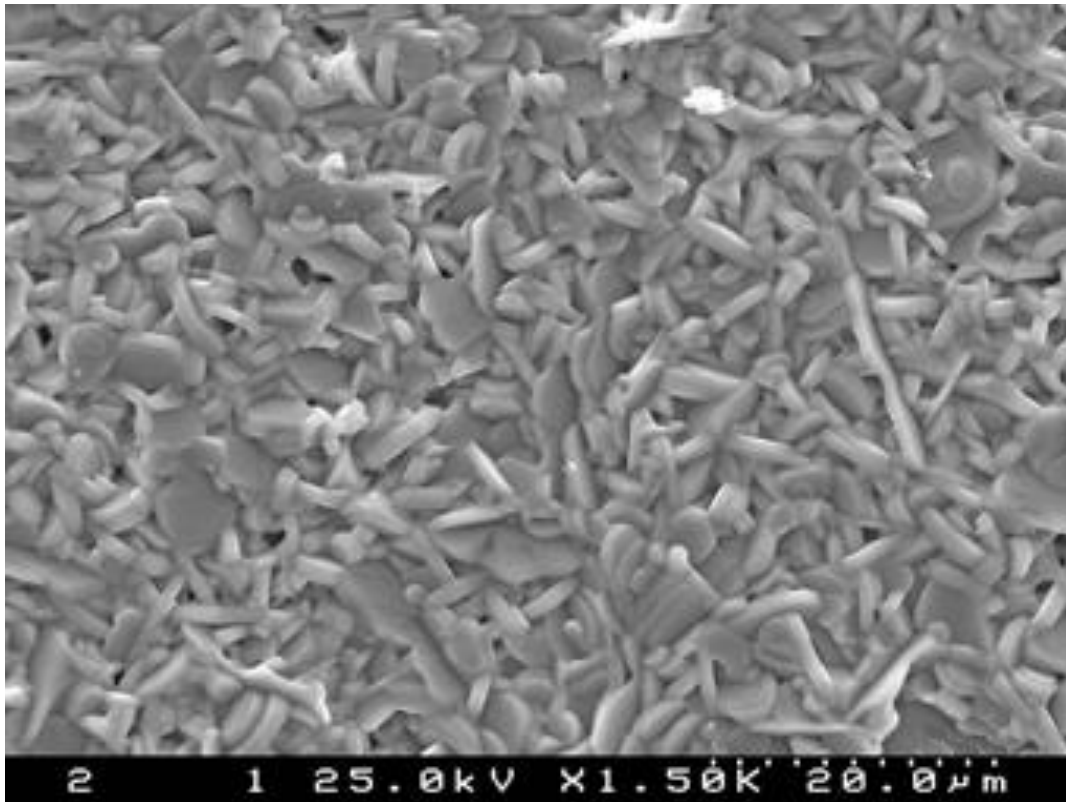
$$u(x) = \frac{\phi(x)}{2\pi g_0}$$

and can be easily determined from the phase term and the frequency of the reference set of fringes. The fringe deformation ($\varepsilon(r)$) can be deduced as follows:

$$\varepsilon(r) = \frac{\delta u(x)}{\delta x} = \frac{\delta}{\delta x} \left[\frac{\phi(x)}{2\pi g_0} \right] \quad [3]$$

Results and discussion

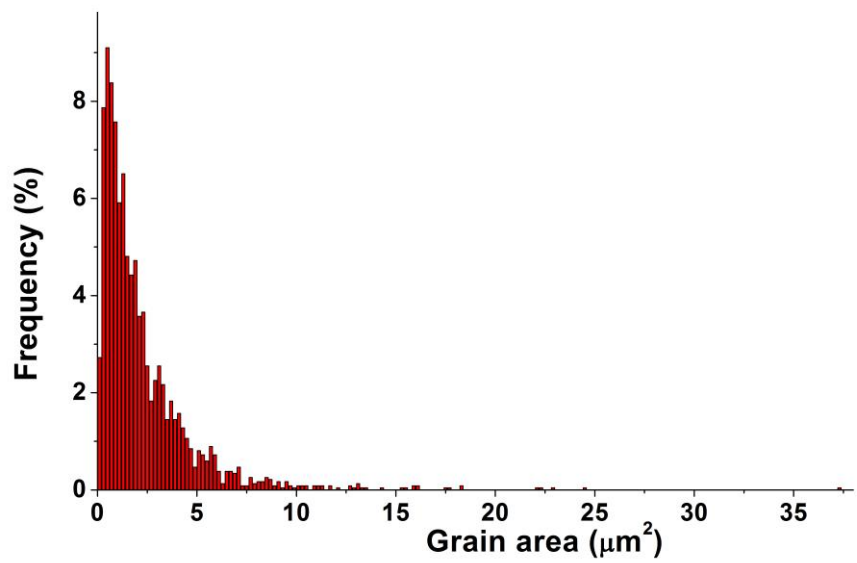
SEM micrographs showing the microstructure of a) CS BLT and b) HP BLT ceramics having similar densities ($96 \pm 1\%$) are shown in Figure 3. It can be observed that few and small pores are remaining after thermal consolidation in both samples and no 2nd phases are discernible, in accordance with previous studies in this system [14]. The differences in grain sizes of both images were quantified using image J and more than 2000 grains were considered for the stereological characterization of each ceramic. The results of the grain size distribution of CS and HP are plotted in Figures 3 c) and d), respectively. A SEM micrograph of higher magnification from HP ceramics is shown in Figure 3 e), highlighting the bimodal characteristics of the microstructures with abnormal grains in a finer grain matrix. Therefore, the grains were classified into two groups, according to the Hillert criterion [17], i.e, grains with size equal or larger than 2.5 times the average grain size are classified into abnormal grains which is equivalent to considering abnormal grains as those with grain area equal or greater than 6.25 times the average grain area, as in the present case.



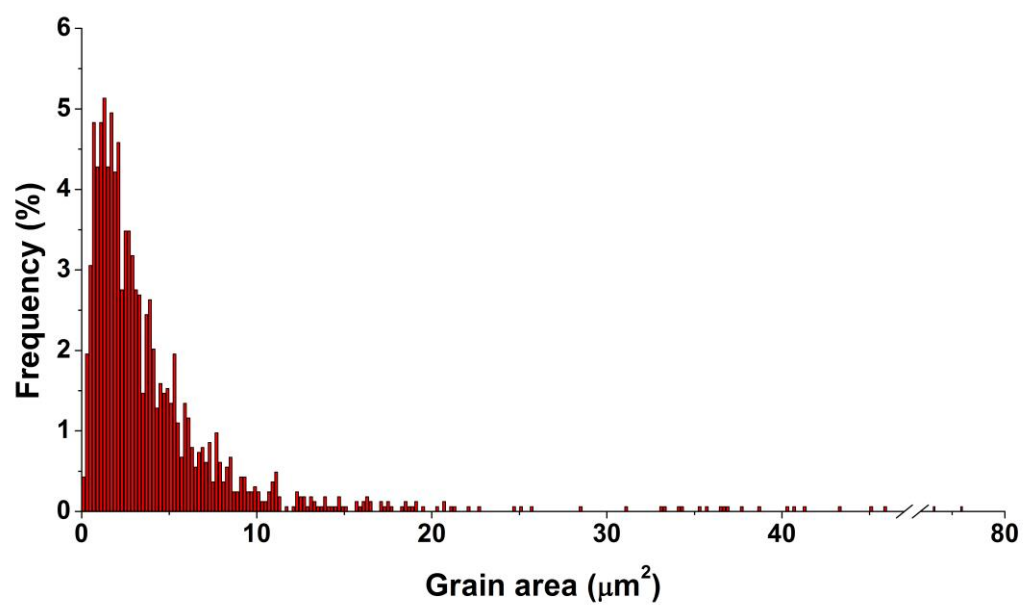
a)



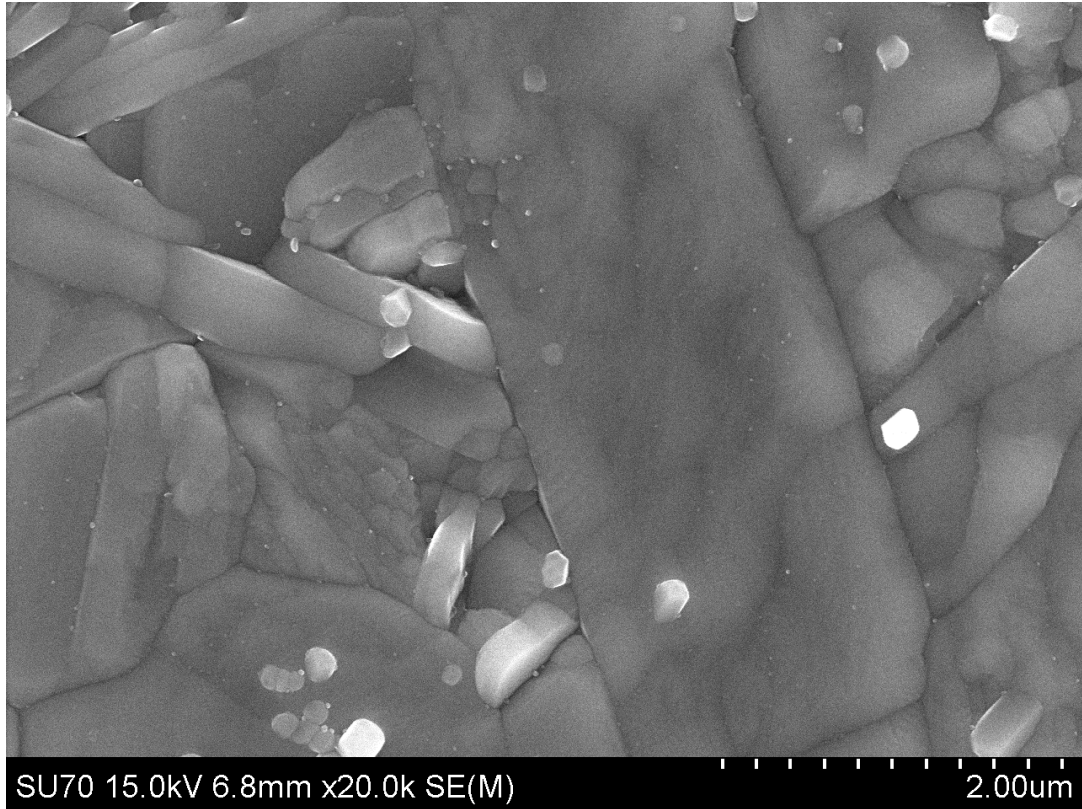
b)



c)



d)



e)

Figure 3. SEM micrographs of a) CS and b) HP BLT ceramics, c) grain size distribution of CS and d) grain size distribution of HP and e) a high magnification image of HP sample showing an abnormal grain into the matrix of thinner grains.

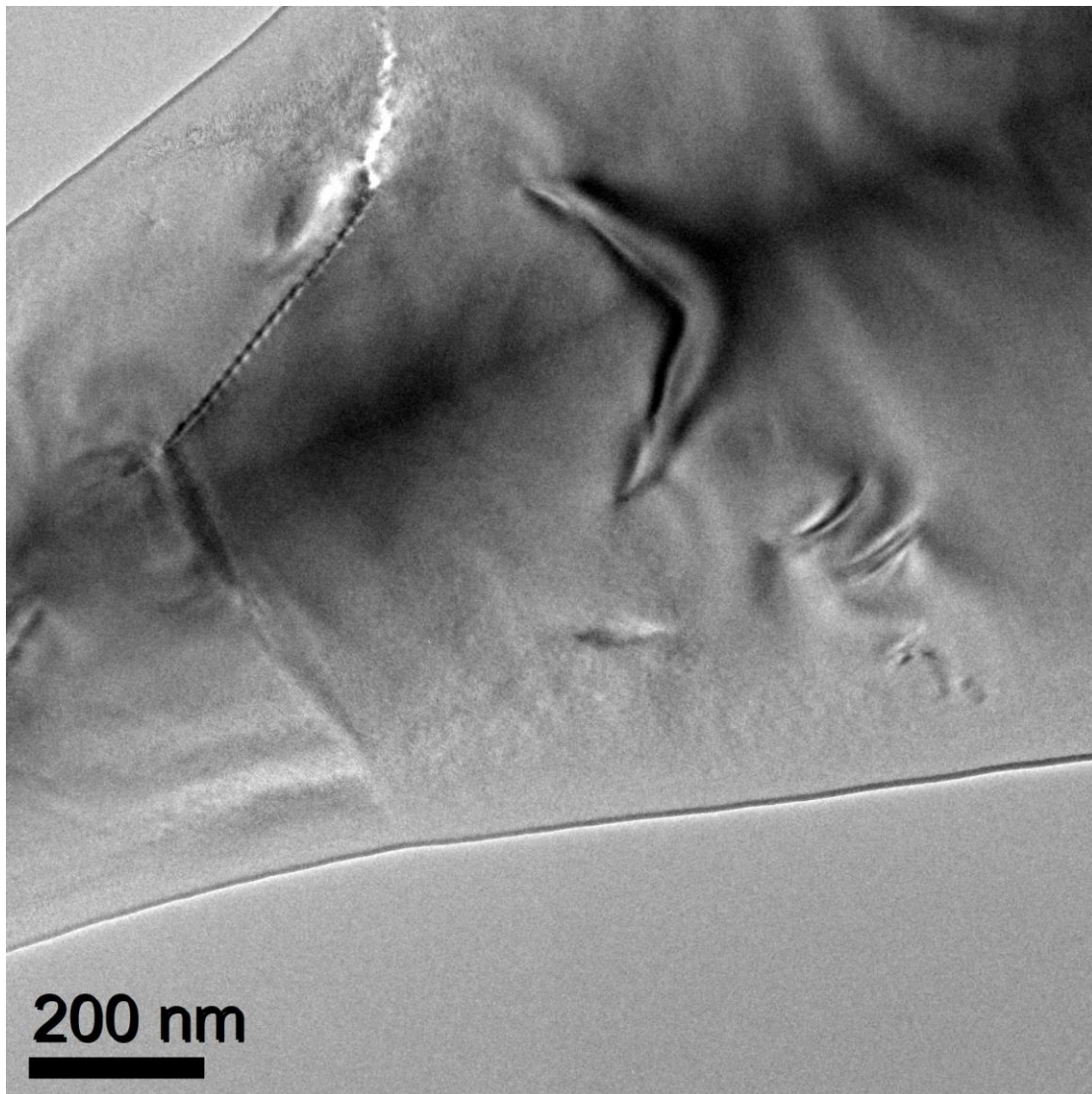
Table 1 reviews the values of the microstructural parameters of HP and CS ceramics. The average grain area of normal grains in CS is $2.0 \mu\text{m}^2$ while that for HP is $3.5 \mu\text{m}^2$. The numeric percentage of abnormal grains and their contribution to the total grain area for CS, are 2.2% and 13%, while those for HP ceramics are 2.8% and 20%, respectively. The difference in the microstructure is clearly visible in the case of the average area of abnormal grains of both ceramics. Abnormal grains in CS have an average area of $13 \mu\text{m}^2$ while that for HP is $30 \mu\text{m}^2$. These data clearly show that an increase in the grain growth was observed in pressure assisted HP, especially in the abnormal grain population, despite the fact that it was sintered at $280 \text{ }^\circ\text{C}$ lower than free sintered CS ceramics. Observation of favoured abnormal grain growth was also reported previously by our group in the constrained sintering of BLT and BNT thick films [15].

Table 1. Microstructural parameters of CS and HP BLT ceramics.

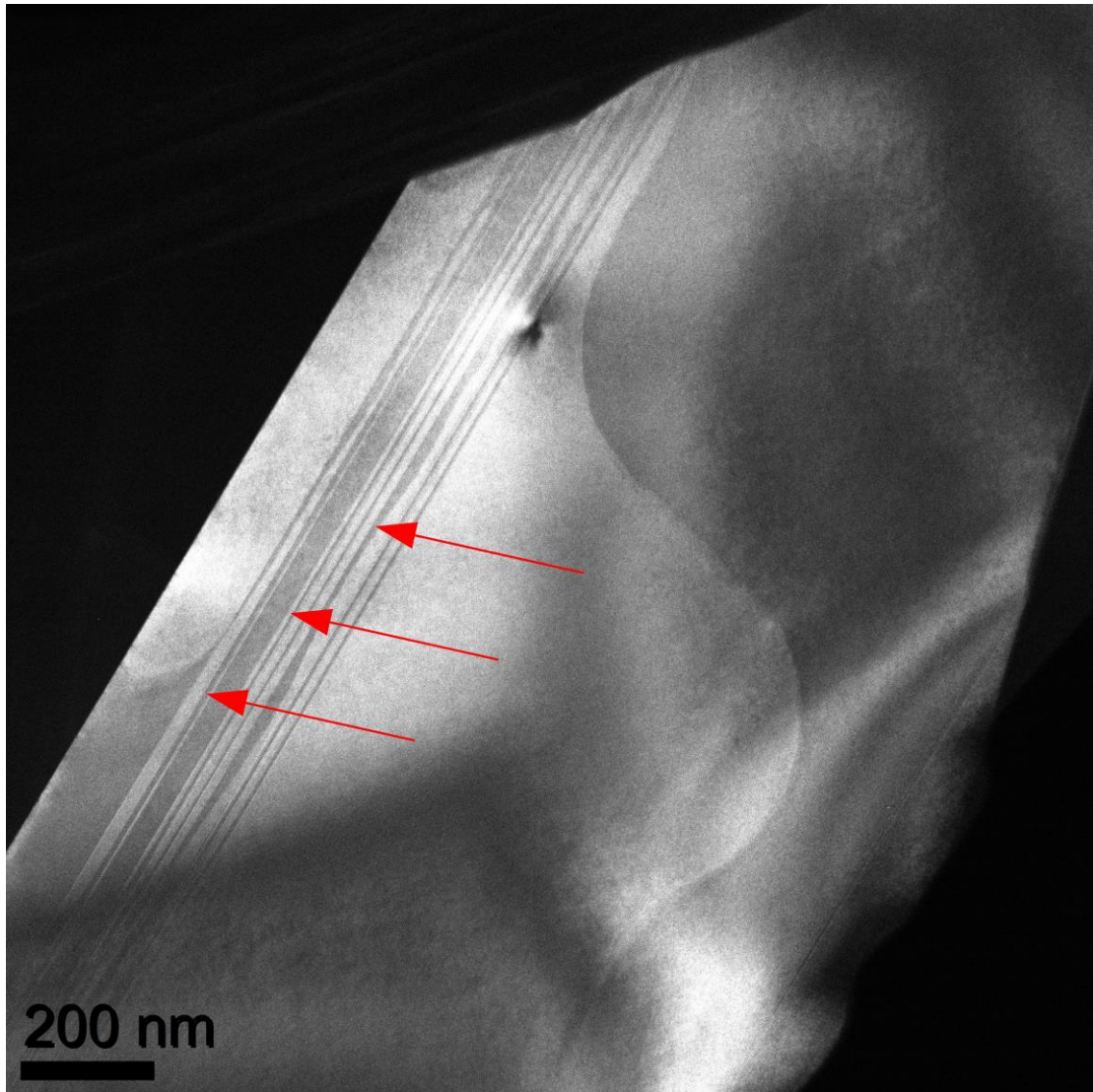
	Density (%)	\bar{A}_{normal}	$\bar{A}_{\text{abnormal}}$	% abnormal	% abnormal
--	-------------	---------------------------	-----------------------------	------------	------------

		(μm^2)	(μm^2)	grains (in area)	grains (in number)
CS	97	2.0	13	13	2.2
HP	96	3.5	30	20	2.8

TEM observations of CS and HP ceramics were first taken at lower magnification and images are shown in Figure 4. In the case of the CS ceramics, Figure 4 a), grains have less imperfections compared to HP. A representative TEM micrograph of HP ceramics is illustrated in Figure 4 b) showing a higher concentration of stacking faults than is usual in layered structures. The density of stacking faults is clearly higher than that observed in CS ceramics and any previously report for BLT [7,8].



a)

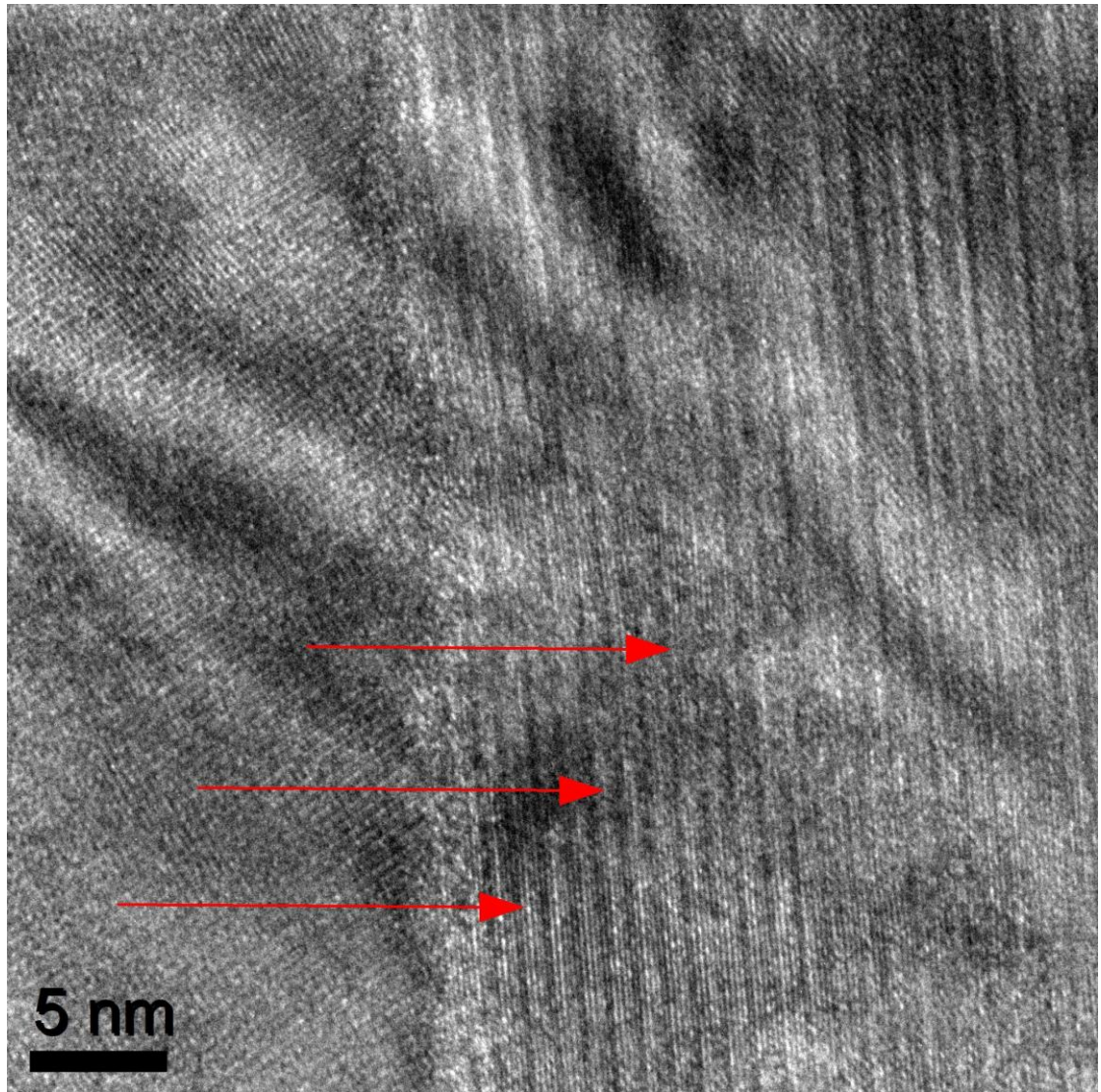


b)

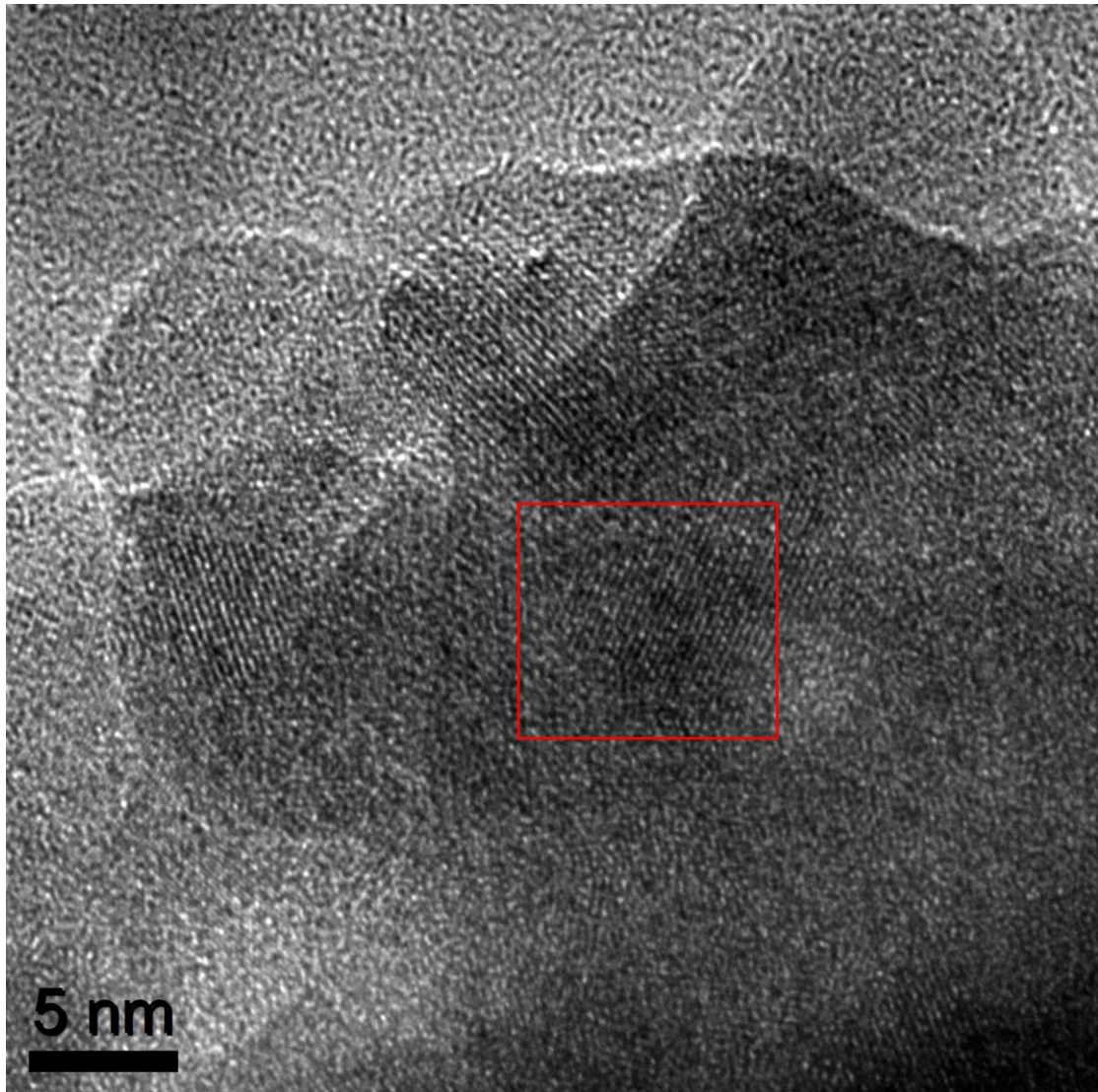
Figure 4. TEM micrographs of BLT ceramics: a) CS with less crystal imperfections and b) HP which shows a higher density of stacking faults (indicated by arrow) and other crystal imperfections when compared with CS ceramics.

To study the effects of external stress at a nanoscale level, HRTEM was used in the bulk and at the GB's. At least 10 images of the interior grain and GB's have been observed for each CS and HP samples **the comparison between CS and HP are consistent in the images which were analysed, also the behaviour is similar in the strain maps as well.** HRTEM images of the HP ceramics exhibited distinct differences from CS ceramics both in bulk and GB's (Figure 5). In Figure 5 a) the HRTEM image of one representative GB of HP ceramics is shown where the defect concentration around this region is clearly visible and in Figure 5 b) the interior grain part of the HP ceramics also shows a higher defect concentration whereas the grains and GB's of the CS ceramics (Figure. 6) do not show evidence of appreciable structural defects.

The higher defect concentration in HP ceramics may arise from the applied pressure during sintering and from this observation we expect that the externally applied sintering pressure is not only responsible for the alterations of the GB characteristics but also for modifications in the interior of the grains.



a)



b)

*Figure 5 HRTEM micrographs of HP ceramics showing defects in two regions
a) in a GB and b) in the bulk (shown in the marked area).*

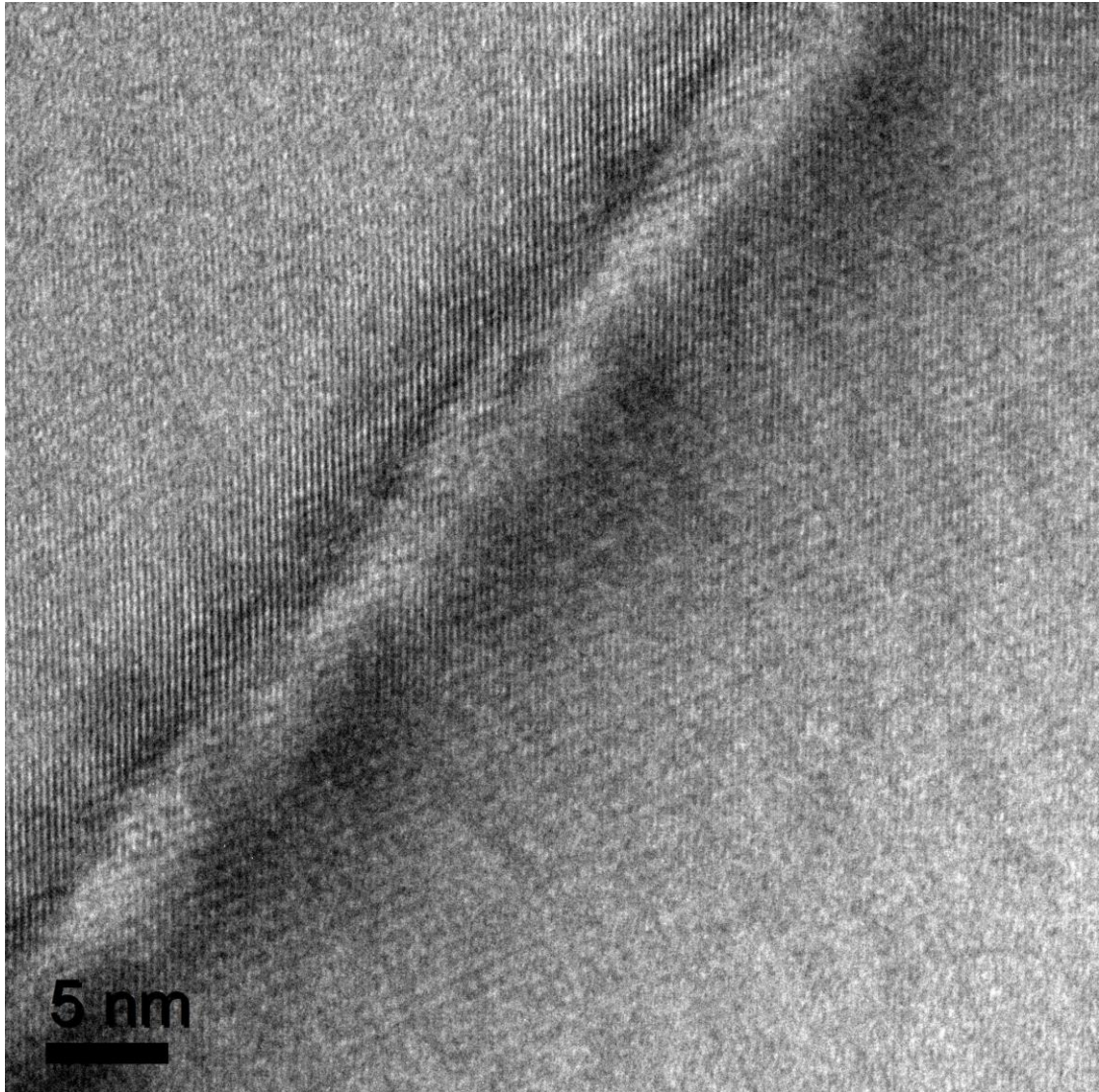


Figure 6: HRTEM micrographs of GB region of a CS BLT ceramics is defect free compared to equivalent region in HP BLT ceramics.

To obtain a more quantitative analysis of the effect of the external applied stress during sintering of BLT on the creation of structural defects, local deformation maps were obtained by GPA for both ceramics. Figure 7 a) depicts a HRTEM micrograph of CS ceramics in GB region. Figure 7 b), c) and d) show the reconstructed phase image, deformation and the rotation maps. The spatial resolution, determined by the size of the mask used in Fourier space (a gaussian mask of $\text{FWHM}=0.5\text{nm}^{-1}$), is 2nm. The background noise was estimated by calculating the standard deviation in a uniform area (indicated by a dashed square in Figure 7 b)). The error bar is $\pm 0.3\%$ for the deformation and $\pm 0.2^\circ$ for the rotation. Average lines profiles extracted from the maps along the rectangles are shown in Figure 7 e) and f). The deformation and the rotation are uniform across the analyzed region of the grain, except at the grain boundaries due to the associated imperfections. The deformation and rotation profiles show only high frequency oscillations

which remain within the noise limits (between $\pm 0.3\%$ and $\pm 0.2^\circ$ respectively). In average the oscillations remain close to zero and therefore no significant deformation is detected.

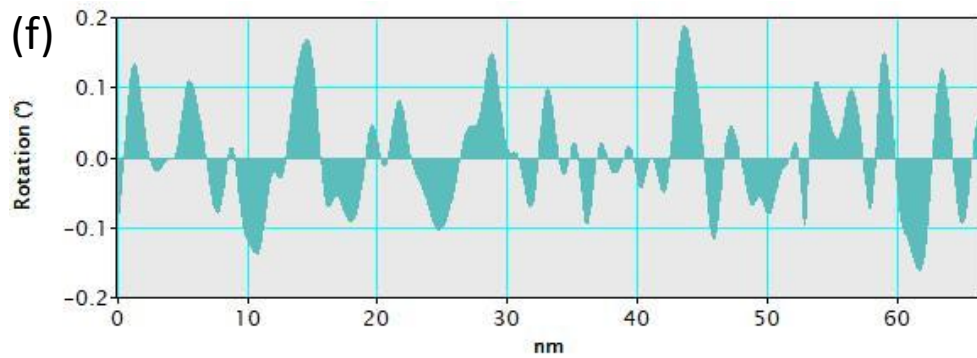
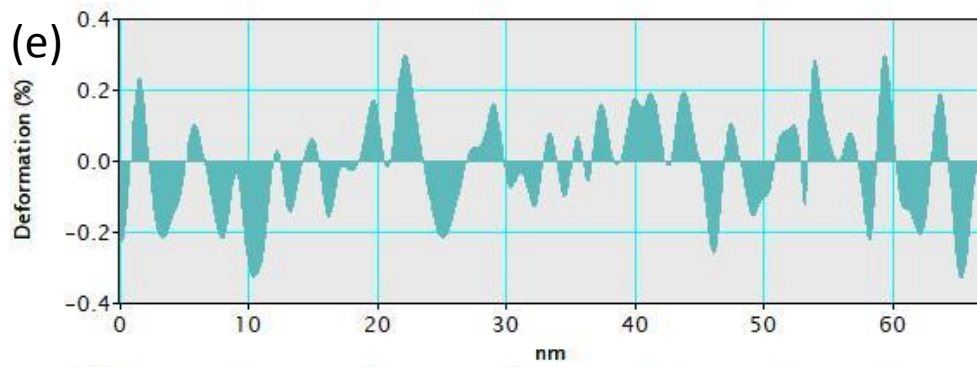
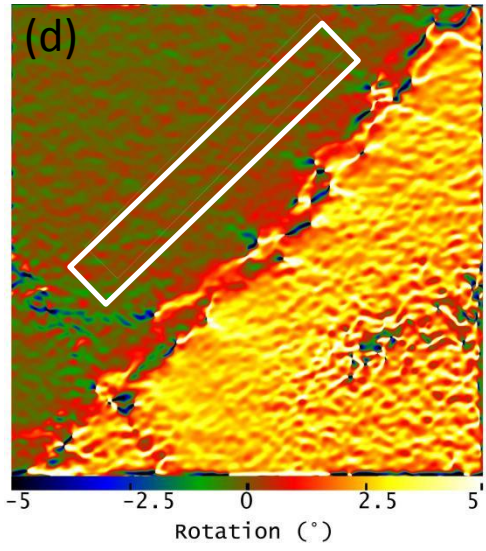
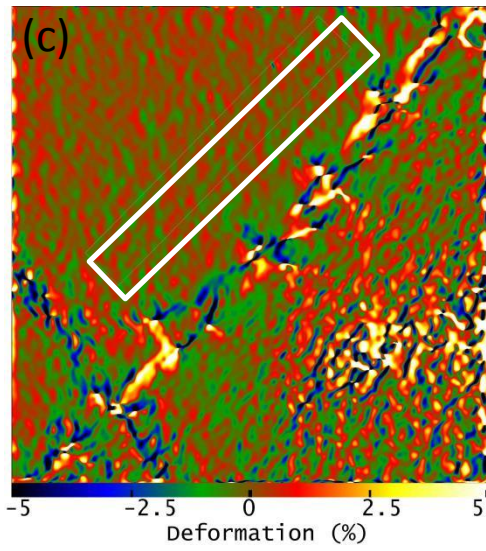
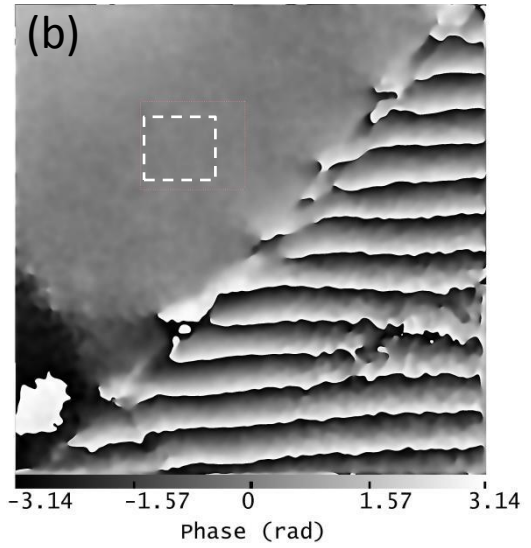
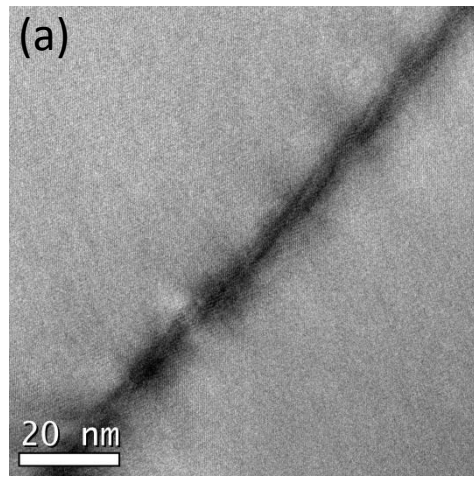


Figure 7- a) HRTEM micrograph of CS BLT ceramics. b) Reconstructed phase image (the dotted rectangle in the phase image indicates the reference region for the deformation). c) Deformation and d) rotation maps calculated using the GPA method . e) Average line profiles of the deformation and f) rotation extracted from the maps according to the white rectangles. GPA analysis suggests no relevant changes in fringe periodicity and rotation of lattices for CS BLT ceramics.

Figure 8 a) shows a HRTEM image of the interior part of a grain in HP BLT ceramics. Phase, deformation and rotation maps determined by GPA are also presented in Fig. 8 b), c) and d). Average line profiles extracted from the maps along the rectangles are shown in Fig. 8 e), f). The deformation is not uniform across the grain and is higher in the top-right region compared to the bottom-left region. In addition, the rotation map shows that there is a gradient of rotation from the bottom-left to the top-right region. The deformation profile shows some variations between -0.4% and up to +0.7% in the top-right corner. The rotation profile shows a linear gradient between -0.5 to +0.5°.

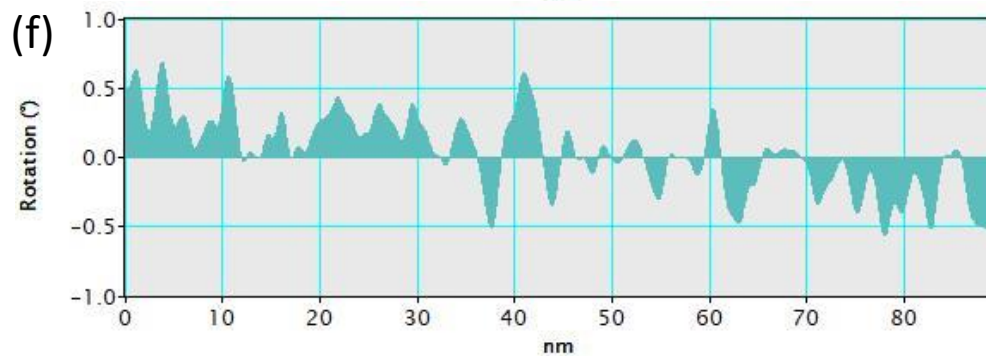
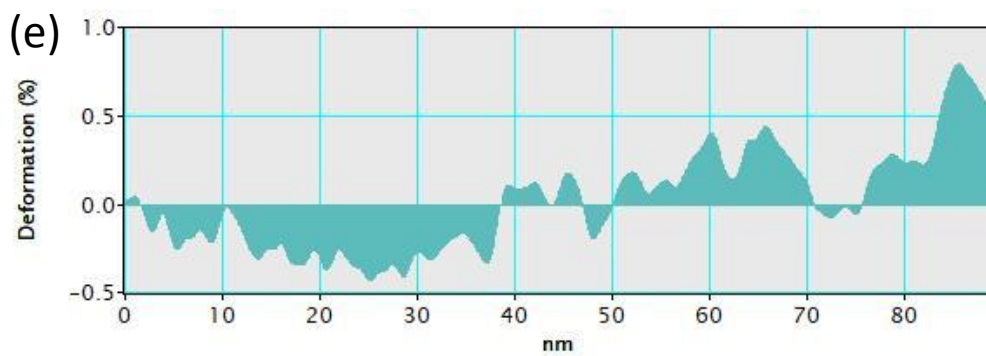
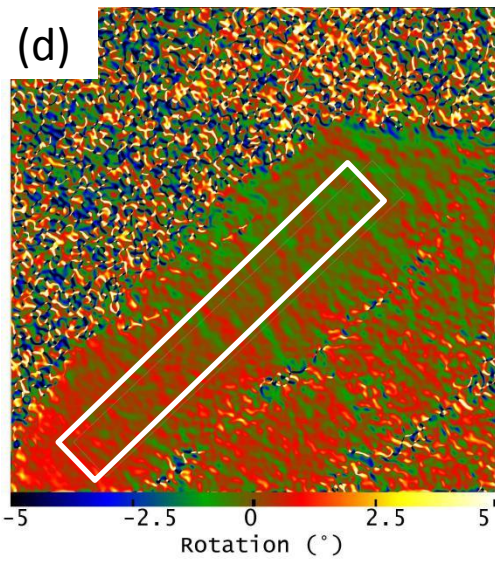
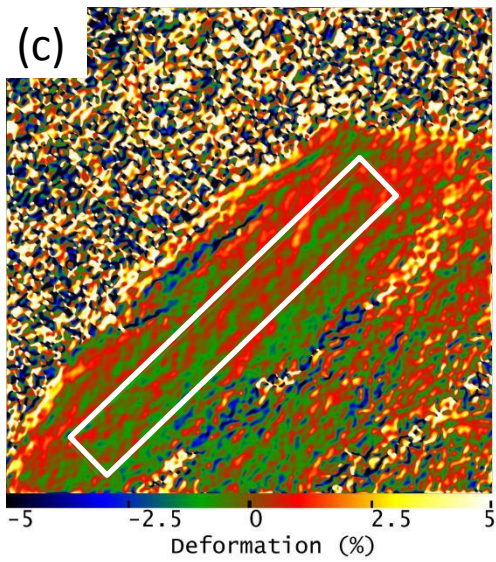
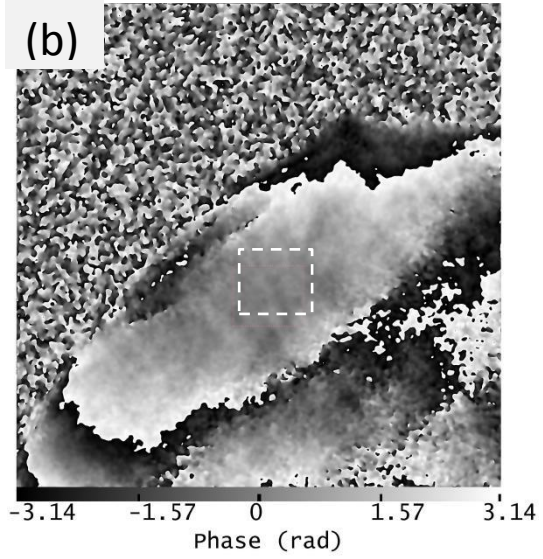
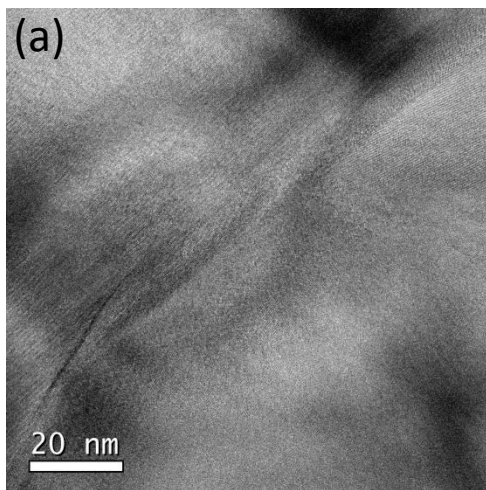


Figure 8- a) HRTEM micrograph of HP BLT ceramics. b) Reconstructed phase image (the dotted rectangle in the phase image indicates the reference region for deformation), c) Deformation and d) rotation maps calculated using the GPA method. e) Average line profiles of the deformation and f) rotation extracted from the maps according to the white rectangles. The maps indicate that the grain contains residual deformations up to 0.7% in the top-right corner and rotations up to 0.5°.

These observations clearly indicate that there are structural changes in BLT arising from the application of external stress during sintering and confirm previous TEM observations (Figure 5 b)) of highly defective structures in HP BLT ceramics.

The reported results clearly show that external stresses during sintering affect the microstructural development at the nanoscale level, being responsible for the creation of higher defective bulk and grain boundary regions. Moreover, the enhanced grain coarsening with a higher contribution of abnormal grain growth in HP ceramics is related to the high structural defects concentration arisen from the applied external stresses during sintering. Observation of high density of stacking faults (which generally arises due to the Ti vacancy layers [7, 8]) indicates that the applied stress is modifying the stacking of AO_3 layers of BLT which in turn creates Ti vacancy layer and stacking faults. Stress assisted sintering has, therefore, the potential to be used as a tool to design microstructures and achieve tailored properties, as suggested from our previous results in BLT and BNT [14, 15].

However, further work is needed to understand how the terms of the GBs velocity are affected, i.e, if, for instances, GB mobility is directly enhanced by the creation of more defective GBs, higher order complexions as in alumina [6] or the driving force is increased by the creation of higher energy GBs [10]. It is also necessary to relate the microstructure variation with the electrical response. It is expected that microstructure changes due to applied pressure may drive a change in τ_f possibly adjustable by the sintering pressure. So HP will provide a way to design temperature compensated microwave materials with a compromise in the quality factor.

Conclusions

The structural changes and the modifications in BLT ceramics due to the external stress applied during sintering were studied using HRTEM and the results were analysed through GPA method. CS BLT ceramics prepared without external applied stress during sintering present minimal or no imperfections in the grain interiors and low defect GBs, while the HP BLT ceramics have a considerable higher density of stacking faults which arises due to the addition or removal of layers or variation of distance between AO_3 mixed layers both in grains interior and GBs; this variation is facilitated by the sintering stress, and these stacking faults drives the anisotropies in the

microstructure of HP BLT. The GPA shows that HP BLT ceramics have fringe deformations as well as rotations; this confirms that the external pressure applied during sintering has a role in modifying the structure and microstructure of BLT material.

Acknowledgments:

The authors acknowledge Fundação para a Ciência e a Tecnologia (FCT), Fundo Europeu de Desenvolvimento Regional Portugal (FEDER), QREN-COMPETE Portugal, the Associate Laboratory CICECO (PEst-C/CTM/LA0011/2013) for funding support. NBS acknowledges FCT for financial support (SFRH/BPD/82158/2011). The authors acknowledge the support of European Union seventh framework programme under a contract for an integrated infrastructure initiative (312483-ESTEEM2).

Data Availability

This work includes mainly "raw" data (eg, as recorded from apparatus) and processed data (eg, as derived from raw data, and/or output from code).

References

- [1] MT Sebastian, H Jantunen, Low loss dielectric materials for LTCC applications: a review, *International Materials Reviews* (2008) 53 (2), 57-90.
- [2] IM Reaney, D Iddles, Microwave dielectric ceramics for resonators and filters in mobile phone networks, *Journal of the American Ceramic Society* (2006) 89 (7), 2063-2072.
- [3] T. M. Hare, H. Palmour III, Effect of Process Optimization Properties of Alumina Sintered Under Rate Control. In *Ceramic Processing Before Firing*; Onoda G. Y., Jr., Hench, L. L., Eds.; John Wiley & Sons Inc.: New York, 1978; pp 307–320.
- [4] C. Genuist, F. J. M. Haussonne, Sintering of BaTiO₃: Dilatometric Analyses of Diffusion Models and Microstructure Control, *Ceram. Int.*, 14 (1988), pp. 169–179.
- [5] L. Amaral, A.M.R. Senos, P.M. Vilarinho, Sintering Kinetic Studies in Nonstoichiometric Strontium Titanate Ceramics, *Mat. Res. Bull.*, 44 (2009), pp. 263-70.
- [6] S. J. Dillon, M. Tang, W. C. Carter, M. P. Harmer, Complexion: A new concept for kinetic engineering in materials science, *Acta Materialia*, 55, 8, (2007), pp. 6208 – 6218.
- [7] H. Zheng, D. Woodward, L. Gillie, I. M. Reaney, Structure and microwave dielectric properties of BaLa₄Ti₄O₁₅, *J. Phys.: Condens. Matter*, 18 (2006), pp. 7051 – 7062.
- [8] N. Harre, D. Mercurio, G. Trolliard, B. Frit, Crystal structure of BaLa₄Ti₄O₁₅, member n= 5 of the homologous series (Ba, La)_nTi_{n-1}O_{3n} of cation deficient perovskite-related compounds, *Materials Research Bulletin*, 33, 10 (1998), pp. 1537 – 1548.

- [9] L. Amaral, M. Fernandes, I. M. Reaney, M. P. Harmer, A. M. R. Senos, P. M. Vilarinho, Grain Growth Anomaly and Dielectric Response in Ti-rich Strontium Titanate Ceramics, *J. Phys. Chem. C*, 117 (2013), pp. 24787 – 24795.
- [10] W. Rheinheimer, M. Baurer, H. Chien, G. S. Rohrer, C. A. Handwerker, J. E. Blendell, M. J. Hoffmann, The equilibrium crystal shape of strontium titanate and its relationship to the grain boundary plane distribution, *Acta Materialia*, 82 (2015), pp. 32 – 40.
- [11] M. Baurer, S. J. Shih, C. Bishop, M. P. Harmer, D. Cockayne, M. J. Hoffmann, Abnormal grain growth in undoped strontium and barium titanate, *Acta Materialia*, 58 (2010), pp. 290 - 300.
- [12] J. H. Haeni, P. Irvin, W. Chang, R. Uecker, P. Reiche, Y. L. Li, S. Choudhury, W. Tian, M. E. Hawley, B. Craigo, A. K. Tagantsev, X. Q. Pan, S. K. Streiffer, L. Q. Chen, S. W. Kirchoefer, J. Levy, D. G. Schlom, Room-temperature ferroelectricity in strained SrTiO₃, *Nature*, 430 (2004), pp. 758 – 761.
- [13] J. Besson, M. Abouaf, Microstructural changes in alumina during hot isostatic pressing, *Mater Sci Eng A*, 109 (1989), pp. 37 - 43.
- [14] J. Besson, M. Abouaf, Grain growth enhancement in alumina during hot isostatic pressing, *Acta Metall Mater*, 39, 10 (1991), pp. 2225 - 2234.
- [15] Zhi Fu, P. M. Vilarinho, A. Wu, A. I. Kingon, Textured Microstructure and Dielectric Properties Relationship of BaNd₂Ti₅O₁₄ Thick Films Prepared by Electrophoretic Deposition, *Advanced Functional Materials*, 19 (2009), pp. 1 – 11.
- [16] L. Amaral, C. Jamin, A. M. R. Senos, P. M. Vilarinho, O. Guillon, Effect of the Substrate on the Constrained Sintering of BaLa₄Ti₄O₁₅ Thick Films, *J. Am. Ceram. Soc.*, 95, 12 (2012), pp. 3781 – 3787.
- [17] M. Hillert, On the theory of normal and abnormal grain growth, *Acta Metall. Mater.*, 13 (1965), pp. 227 – 238.
- [18] M. J. Hytch, P. Hawkes Ed., Scanning Microscopy Suppl. 10, *Signal and Image in Microscopy and Microanalyses*, 1997.
- [19] M. J. Hytch, Analysis of variations in structure from high resolution electron microscope images by combining real space and Fourier space information, *Microsc. Microanal. Microstruct.*, 8 (1997), pp. 41 – 57.
- [20] M. J. Hytch, L. Potez, Geometric phase analysis of high resolution electron microscopy images of antiphase domains: example Cu₃Au, *Philos. Mag.*, 76 (1997), pp. 1119 – 1138.
- [21] M. J. Hytch, P. Bayle, Analysis of the variation of individual image periodicities across a strained metal multilayer, *Proc. ICEM 13th Editions de Physique*, Paris, A 2, (1994), pp 129-130.
- [22] M. J. Hytch, E. Snoeck, R. Kilaas, Quantitative measurement of displacement and strain fields from HREM micrographs, *Ultramicroscopy*, 74 (1998), pp. 131 - 146.

[23] J.-M. Zuo, A. B. Shah, H. Kim, Y. Meng, W. Gao, J.-L. Rouvière, Lattice and strain analysis of atomic resolution Z-contrast images based on template matching., *Ultramicroscopy* 136 (2014) 50–60.

Figure captions

Figure. 1 Schematic representation of the layered perovskite structure of BLT in which A represents Ba and La ions in the structure [7,8]. The BLT structure exhibits some layers in which the octahedra are face rather than corner shared [7].

Figure 2. Schematic of the preparation of HP BLT ceramics.

Figure 3. SEM micrographs of a) CS and b) HP BLT ceramics, c) grain size distribution of CS and d) grain size distribution of HP and e) a high magnification image of HP sample showing an abnormal grain into the matrix of thinner grains.

Figure 4. TEM micrographs of BLT ceramics: a) CS with less crystal imperfections and b) HP which shows a higher density of stacking faults (indicated by arrow) and other crystal imperfections when compared with CS ceramics.

Figure 5 HRTEM micrographs of HP ceramics showing defects in two regions a) in a GB and b) in the bulk (shown in the marked area).

Figure 6. HRTEM micrographs of GB region of a CS BLT ceramics is defect free compared to equivalent region in HP BLT ceramics.

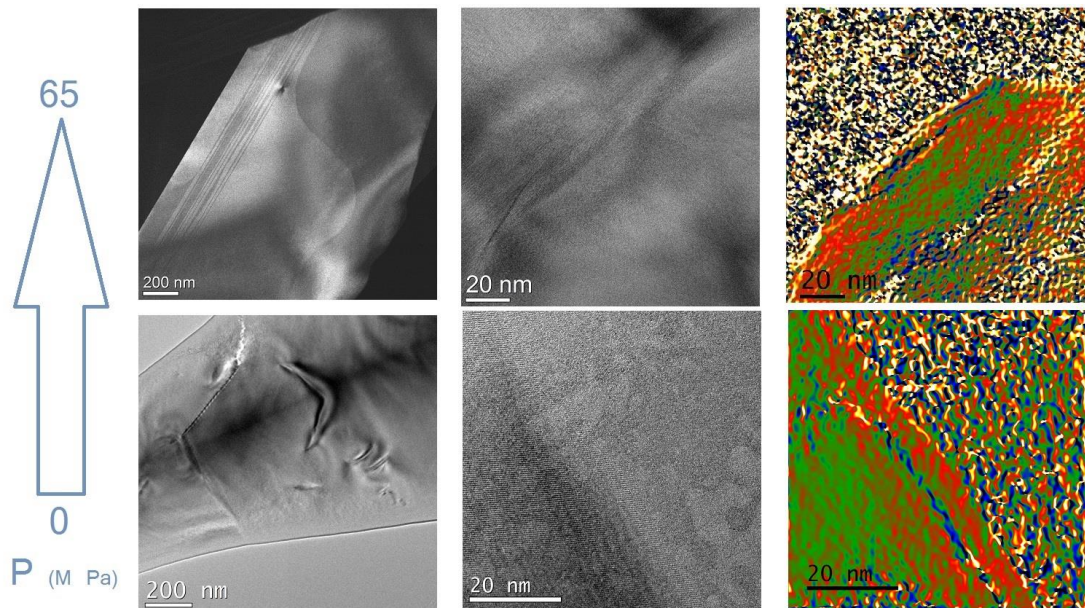
Figure 7- a) HRTEM micrograph of CS BLT ceramics. b) Reconstructed phase image (the dotted rectangle in the phase image indicates the reference region for the deformation). c) Deformation and d) rotation maps calculated using the GPA method. e) Average line profiles of the deformation and f) rotation extracted from the maps according to the white rectangles. GPA analysis suggests no big changes in fringe periodicity and rotation of lattices for CS BLT ceramics.

Figure 8- a) HRTEM micrograph of HP BLT ceramics. b) Reconstructed phase image (the dotted rectangle in the phase image indicates the reference region for deformation), c) Deformation and d) rotation maps calculated using the GPA method. e) Average line profiles of the deformation and f) rotation extracted from the maps according to the white rectangles. The maps indicate that the grain contains residual deformations up to 0.7% in the top-right corner and rotations up to 0.5°.

Tables

Table 1. Microstructural parameters of CS and HP BLT ceramics.

Graphical Abstract



A novel defect creation mechanism originated due to the externally applied sintering pressure is reported and analysed using HRTEM and geometrical phase analysis (GPA).